NASA TECHNICAL NOTE

NASA TN D-2241

NASA TN D-2241

COMPARISON OF FLIGHT PRESSURE MEASUREMENTS WITH WIND-TUNNEL DATA AND THEORY FOR THE FORWARD FUSELAGE OF THE X-15 AIRPLANE AT MACH NUMBERS FROM 0.8 TO 6.0

by Jon S. Pyle

Flight Research Center
Edwards, Calif.

NATIONAL AERONAUTICS AND SPACE ADMINISTRATION • WASHINGTON, D. C. • JANUARY 1964

COMPARISON OF FLIGHT PRESSURE MEASUREMENTS WITH WIND-TUNNEL DATA AND THEORY FOR THE FORWARD FUSELAGE OF THE X-15 AIRPLANE AT MACH NUMBERS FROM 0.8 TO 6.0

By Jon S. Pyle

Flight Research Center
Edwards, Calif.

NATIONAL AERONAUTICS AND SPACE ADMINISTRATION

For sale by the Office of Technical Services, Department of Commerce,
Washington, D.C. 20230 -- Price $0.75

COMPARISON OF FLIGHT PRESSURE MEASUREMENTS WITH WIND-TUNNEL DATA AND THEORY FOR THE FORWARD FUSELAGE OF THE X-15 AIRPLANE AT MACH NUMBERS FROM 0.8 TO 6.0

By Jon S. Pyle

SUMMARY

The results of flight pressure measurements on the forward fuselage of the X-15 airplane are presented for angles of attack from 0° to 15° and Mach numbers from 0.8 to 6.0.

Comparisons of flight and wind-tunnel data showed good agreement, and theoretical calculations predicted flight pressure measurements reasonably well.

INTRODUCTION

The design of an aerospace vehicle which must maneuver in the atmosphere is subject to the magnitude and distribution of aerodynamic forces. In addition, during reentry maneuvers or at high supersonic Mach numbers, a knowledge of surface pressures is important in determining heating rates. Notable advances in the knowledge of flight surface pressures were made with the early NACA research aircraft, such as the X-1, D-558-II, and the X-1E (refs. 1, 2, and 3, respectively). In the more recent X-15 research program, this capability has been extended from the subsonic, transonic, and low supersonic environments of the earlier aircraft to the high supersonic region.

This paper presents the results of flight-test measurements of surface pressures over the forward axially symmetric portion of the X-15 fuselage for Mach numbers extending to approximately 6.0 and angles of attack to 15°. Flight data are compared with the results from wind-tunnel tests (refs. 4 and 5) and from theoretical predictions (refs. 6 to 9). Both chordwise and radial pressure distributions are presented for the forebody section, including centerline distributions along the canopy.

SYMBOLS

C_p pressure coefficient, $\frac{p - p_\infty}{q}$

l	overall fuselage length, ft
M	free-stream Mach number
p	local static pressure, lb/sq ft absolute
p_∞	free-stream static pressure, lb/sq ft absolute
q	free-stream dynamic pressure, lb/sq ft absolute
x	distance from nose of fuselage parallel to fuselage centerline, ft
α	angle of attack, deg
β	angle of sideslip, deg
φ	angular location of fuselage orifices measured counterclockwise from bottom centerline of fuselage when facing forward, deg

DESCRIPTION OF AIRPLANE

Three aerodynamically identical X-15 research airplanes were designed and constructed by North American Aviation, Inc., in a program sponsored jointly by the U.S. Air Force, the U.S. Navy, and the National Aeronautics and Space Administration. The airplanes are powered by Reaction Motors YLR99-RM-1 single-chamber rocket engines and are designed to attain speeds up to 6,600 ft/sec or altitudes of 250,000 feet or greater. However, the maximum altitude attained, to date, of 354,200 feet is more than 100,000 feet above design limit, and the maximum speed achieved, over 6,000 ft/sec, is about equal to the design value when adjusted for the increase in airplane weight that occurred during development. Photographs of the airplane are presented in figures 1(a) and 1(b). A three-view drawing is presented in figure 2.

The X-15 fuselage is an axially symmetric body of revolution with a fineness ratio of 10.91. The airplane is 49.17 feet long (see fig. 2). The maximum width (including side fairings) and depth are 7.33 feet and 4.67 feet, respectively. The Nortronics 6.5-inch-diameter spherical airflow sensor, at the fuselage apex, is faired to a 14.75° cone which extends to 3 percent of the fuselage length. The cone, in turn, is tangent to an ogive contour having a radius of 700 inches which extends to 32-percent fuselage length, where it is tangent to a 28-inch-radius cylinder. The cylinder extends over the remainder of the fuselage and has a short boattail section at the engine nozzle.

INSTRUMENTATION

Pressure orifices on all three X-15 airplanes are at identical locations. The orifice locations are listed in table I and shown in figure 3.

All measurements presented in this paper were recorded on NACA 24-cell mechanical manometers mounted in the instrument compartment and referenced to the cabin compartment. Time histories of the pressure variations and parameters were synchronized by a common timer. Angle of attack and angle of sideslip were obtained from the airflow-direction sensor at the fuselage nose. Ambient pressure, Mach number, and altitude used in defining parameters for pressure measurements were obtained by radar and rawinsonde instruments (ref. 10).

Titanium mountings, of 1/4-inch inner diameter, flush with the outer skin served as orifices. Each orifice was connected to the instrument compartment by means of 1/4-inch-inner-diameter aluminum tubing and special high-temperature rubber connectors. Lengths of tubing from orifice to manometer ranged from 5 feet to 20 feet. Lag in the system under relatively steady-state conditions was shown by actual measurement to be negligible.

The estimated overall errors for the quantities measured are as follows:

Mach number	±0.10
Pressure coefficient . . .	±0.02
Angle of attack	±0.75°
Angle of sideslip	±0.75°

TESTS

All data were obtained below an altitude of 100,000 feet and under approximately steady-state conditions. In general, data were chosen from time intervals in which the dynamic pressure was equal to or greater than 500 lb/sq ft. However, at lower Mach numbers where the amount of data available was limited dynamic pressures less than 500 lb/sq ft were used occasionally.

Because of manometer limitations, only 24 (solid symbols, fig. 3) of the 39 orifices on the forward fuselage were used to obtain pressure measurements for this paper. All of the 24 orifices were not connected on every flight, however, since the number of recording channels available for this study varied from flight to flight.

RESULTS AND DISCUSSION

Forebody Pressure Distributions

Surface pressure distributions along the axis of the fuselage are presented and compared with wind-tunnel results (refs. 4 and 5) in figure 4 for the bottom, side, and top centerlines. Angle of sideslip is limited to ±1°, unless otherwise stated. Where wind-tunnel results were not available, flight data were faired with solid lines to indicate the shape of the pressure distributions.

In general, the pressure distributions for the various Mach numbers follow a pattern typical of ogive bodies. At low Mach numbers (figs. 4(a) and 4(b))

the flow around the forebody expands somewhat more abruptly than at supersonic speeds (figs. 4(f) to 4(l)). At transonic speeds (figs. 4(b) and 4(c)), pronounced pressure variations occur over the canopy as a result of strong local shocks. The vertical fairings at 13-percent and 19-percent fuselage length represent an immediate compression and expansion as the flow is deflected over the faceplate of the canopy.

In general, the flight data agree well with the wind-tunnel results. Discrepancies are noted, however, where the flow passes over the two back orifices (28-percent and 32-percent fuselage length) on the canopy at transonic Mach numbers. These differences are believed to be caused by the bug-eye camera fairings on the flight research vehicle that were not included on the wind-tunnel model. Also, at transonic speeds a pitot tube (see figs. 1(a) and 1(b)) extending above the orifice at 12-percent fuselage length on the upper centerline ($\varphi = 180°$) causes interference effects.

Effect of Mach Number

The effect of Mach number on the pressure coefficients at three bottom centerline stations is presented in figure 5. Wind-tunnel and theoretical results are included for comparison.

Considerable scatter is evident in the flight data in figures 5 to 7, particularly at transonic speeds where dynamic pressures were generally below 500 lb/sq ft. The scatter is attributed largely to variations in angle of attack in the ranges shown and, at transonic speeds, to the reduced accuracy of the data for the lower dynamic pressures. For clarity, faired (solid) lines have been drawn through the data points.

Particularly noteworthy in figures 5 to 7 is the sharp rise in pressure coefficient as the airplane passes through the transonic range. In general, the flight measurements and the wind-tunnel results agree well.

For supersonic Mach numbers above 2.0 in figures 5 and 6, theories are presented which generally approximate the flight and wind-tunnel results for the angles of attack shown. It is seen that the Newtonian theory (ref. 8) gives close approximations, but shows no change with Mach number. The unyawed[1] tangent-cone theory gives appropriate variations with Mach number, although the predictions from the unyawed theory are generally high.

Results for a zero angle-of-attack condition are presented in figure 6. Since zero angle-of-attack data at transonic speeds are extremely limited for the X-15 airplane, data are shown for the side centerline ($\varphi = 90°$) of the fuselage at essentially zero sideslip angles. These data at small angles of attack are, thus, representative of the characteristics of the bottom centerline ($\varphi = 0°$) at zero angle of attack. The validity of this approximation may be seen in the comparison of wind-tunnel results for the two conditions presented in figure 6.

[1]Unyawed tangent cone refers to semivertex angles of cones tangent to points on the body, plus angles of attack from charts at zero angle of attack (ref. 9).

The 8-percent fuselage length orifice was used in figure 6 in place of the orifice at 12-percent fuselage length because of the greater amount of data available from the 8-percent location. This orifice was used throughout the flight program as the alternate static source for the velocity and altitude indicator.

The results from linear theory (refs. 6 and 7) and the theories presented in figure 5 are included in figure 6 for comparison with flight and wind-tunnel data. (Subsonic linear theory for the 8-percent fuselage location is equal to a zero pressure coefficient.) All theories except Newtonian are limited to semi-vertex cone angles of about 10°, although the tangent-cone angles of the X-15 fuselage vary between 15° and 5°. In general, the agreement between the flight and wind-tunnel results is good and theoretical predictions are fair.

Effect of Canopy

Protuberances on high-speed bodies often give rise to unpredictable flow effects. Pressure distributions for the centerline of the X-15 canopy are presented in figure 7 for two angle-of-attack ranges over the Mach number range investigated. Sharp transonic flow expansions are noted at the two forward orifices. The presence of a strong local shock at the top of the canopy is shown by the abrupt changes in pressure between the second and third orifices. This shock passes over the third orifice (28-percent fuselage length) at a Mach number of about 1.9 for an angle of attack of about 5°, and a Mach number of 1.5 for an angle of attack of about 10°.

The wind-tunnel and flight-test results are generally in accord except in the transonic range at the two rear canopy orifices. These differences may be due to an interference effect from the flight-vehicle bug-eye camera fairings on each side of the orifices.

The wind-tunnel results at transonic speeds are omitted for the 19-percent location. The orifice location on the wind-tunnel model was not the same as on the flight vehicle; hence, an accurate comparison could not be made where rapid transonic pressure changes occur. At supersonic speeds, however, the pressures are seen to be much less sensitive to Mach number changes; thus, wind-tunnel data could be readily interpolated.

Figure 8 shows the canopy pressure distributions in the transonic range as determined from crossplots of faired pressure coefficients in figure 7. Rather abrupt changes in the pressure distributions occur as the local canopy shock passes over the second orifice at the 22.5-percent fuselage length. These effects begin to appear between Mach numbers of 0.6 and 0.7 at an angle of attack of 5° (fig. 8(a)) and between Mach numbers of 0.8 and 0.9 at an angle of attack of 10° (fig. 8(b)). Corresponding variations are also evident in the vicinity of the orifice at the 28-percent location.

Radial Pressure Distributions

The flight and wind-tunnel results for the radial pressure distributions are shown in figure 9 for Mach numbers from 0.6 to 5.5 and angles of attack from 0° to 15°. Because of the difference in orifice locations between the model and the test airplane, interpolated wind-tunnel results are presented for comparison at the Mach numbers for which wind-tunnel results were available. In general, the comparison shows good agreement.

As expected, pressure coefficients at angles of attack above 0° generally decrease with increasing radial angle with the exception of the orifice at $\varphi = 180°$ which shows interference effects caused by the pitot tube. As angle of attack is increased, the pressure coefficient increases on the lower surface and decreases on the upper surface.

The results of Newtonian theory (ref. 8) are compared with flight and wind-tunnel data at four angles of attack in figure 10. Flight data are shown for Mach numbers of 4.7, 5.0, and 5.5 and wind-tunnel data for a Mach number of 4.7. Although the Newtonian theory is based on high angles of attack and high Mach numbers, it gives reasonable predictions for low angles of attack and for the Mach numbers shown.

The effects of sideslip on the radial pressure distributions are presented in figure 11 for a limited number of conditions for which reliable data are available. As expected, the effects of sideslip are most pronounced near the orifices at the 90° radial positions. The flight and wind-tunnel results for zero sideslip are in good agreement.

CONCLUSIONS

Results obtained from flight surface pressure measurements over the forward fuselage of the X-15 airplane at Mach numbers from 0.8 to 6.0 and angles of attack from 0° to 15° indicate that:

1. Flight and wind-tunnel data agree well.

2. Reasonably accurate approximations of flight values can be made with simple linear, tangent-cone, and Newtonian theories.

Flight Research Center,
National Aeronautics and Space Administration,
Edwards, Calif., November 6, 1963.

REFERENCES

1. Knapp, Ronald J., Jordan, Gareth H., and Johnson, Wallace E.: Fuselage Pressures Measured on the Bell X-1 Research Airplane in Transonic Flight. NACA RM L53I15, 1953.

2. Taillon, Norman V.: An Analysis of Surface Pressures and Aerodynamic Load Distribution Over the Swept Wing of the Douglas D-558-II Research Airplane at Mach Numbers From 0.73 to 1.73. NACA RM H58A30, 1958.

3. Taillon, Norman V.: Flow Characteristics About Two Thin Wings of Low Aspect Ratio Determined From Surface Pressure Measurements Obtained in Flight at Mach Numbers From 0.73 to 1.90. NASA Memo 5-1-59H, 1959.

4. Osborne, Robert S., and Stafford, Virginia C.: Basic Pressure Measurements on a 0.0667-Scale Model of the North American X-15 Research Airplane at Transonic Speeds. NASA TM X-344, 1960.

5. Hodge, B. Leon, and Burbank, Paige B.: Pressure Distribution of a 0.0667-Scale Model of the X-15 Airplane for an Angle-of-Attack Range of 0° to 28° at Mach Numbers of 2.30, 2.88, and 4.65. NASA TM X-275, 1960.

6. Shapiro, Ascher H.: The Dynamics and Thermodynamics of Compressible Fluid Flow. Vol. I, The Ronald Press Co., 1953.

7. Shapiro, Ascher H.: The Dynamics and Thermodynamics of Compressible Fluid Flow. Vol. II, The Ronald Press Co., 1954.

8. Grimminger, G., Williams, E. P., and Young G. B. W.: Lift on Inclined Bodies of Revolution in Hypersonic Flow. Jour. Aero. Sci., vol. 17, no. 11, Nov. 1950, pp. 675-690.

9. Ames Research Staff: Equations, Tables, and Charts for Compressible Flow. NACA Rep. 1135, 1953. (Supersedes NACA TN 1428.)

10. Larson, Terry J., and Webb, Lannie D.: Calibrations and Comparisons of Pressure-Type Airspeed-Altitude Systems of the X-15 Airplane From Subsonic to High Supersonic Speeds. NASA TN D-1724, 1963.

TABLE I

SURFACE PRESSURE-ORIFICE LOCATIONS ON THE FUSELAGE OF THE X-15 AIRPLANE[1]

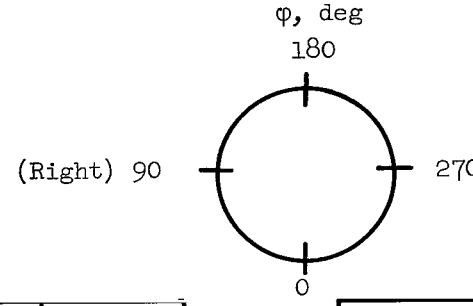

Orifice number	φ, deg	Fuselage station, in.	Percent fuselage length, x/l
03002	0	25	4.2
03003	90		
03004	180		
03005	270		
04001	0	50	8.5
04002	180		
05002	0	71	12.0
05003	22.5		
05004	45		
05005	67.5		
05006	90		
05007	112.5		
05008	135		
05009	157.5		
05010	180		
05011	270		
05012	0	114	19.3
05013	90		
05014	180		
05015	270		

Orifice number	φ, deg	Fuselage station, in.	Percent fuselage length, x/l
05016	0	136	23
05017	180	133	22.5
05018	45	157	26.6
05019	90	167	28.3
05020	180		
05021	270		
05022	0	190	32.2
05023	90		
05024	180	192	32.5
05025	270	190	32.2
05026	315		
09002	0	342.5	58.1
09003	45		
09004	135		
09005	180		
09006	Side fairing top		
09007			
09008	Side fairing bottom		
09009			

[1]The location of each orifice is illustrated in figure 3.

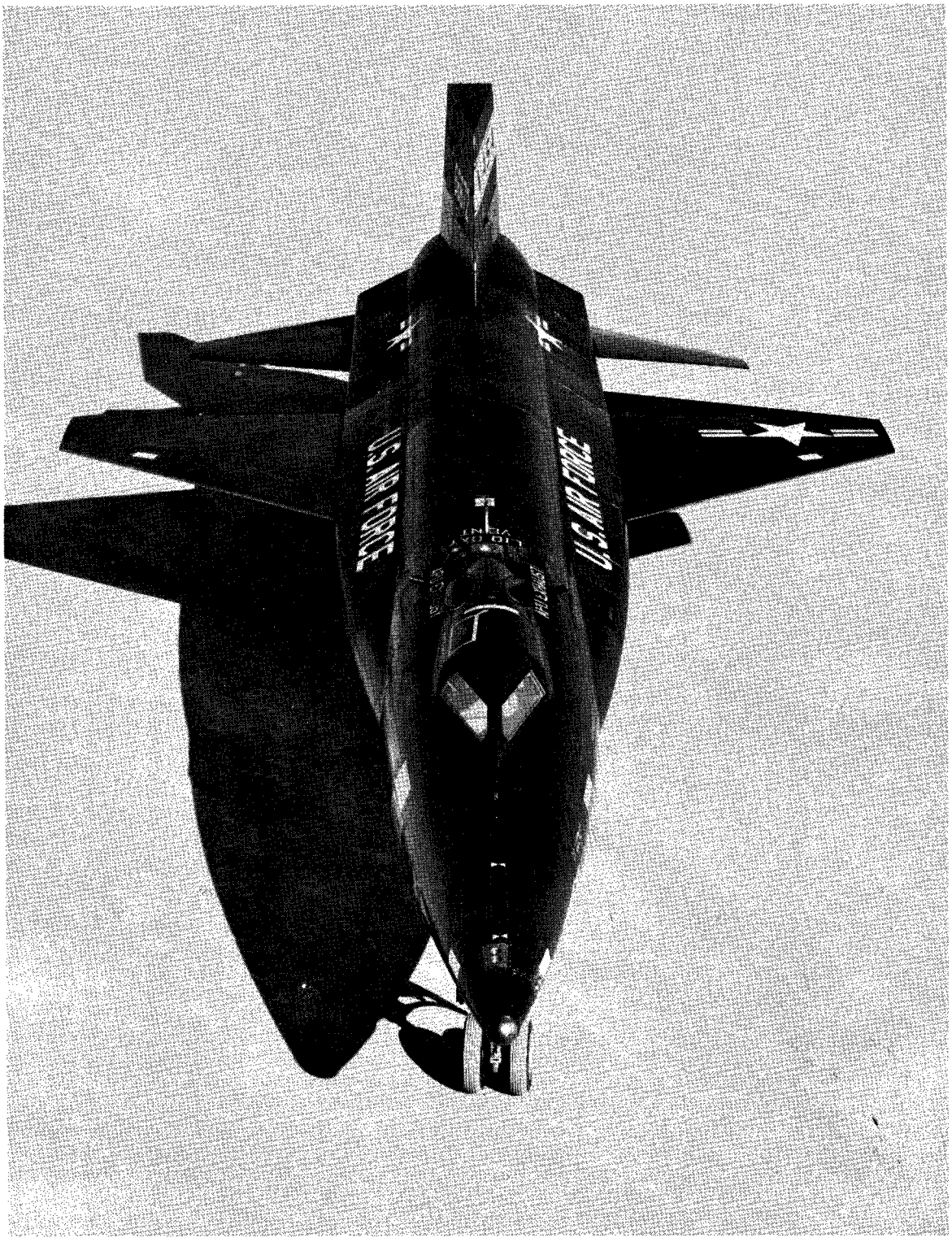

(a) Top view of fuselage forebody.

Figure 1.- X-15 airplane.

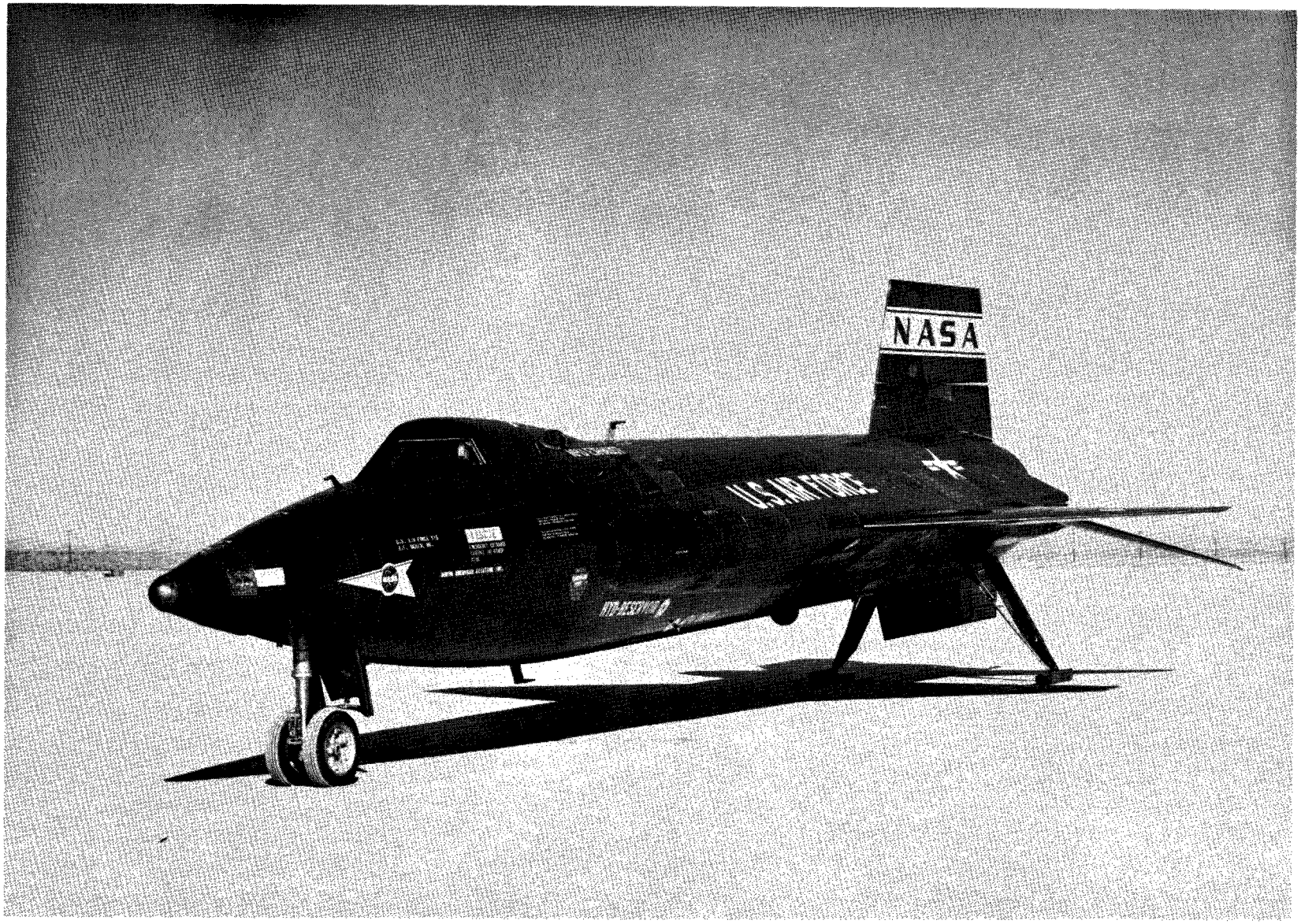

(b) Side view of fuselage forebody.

Figure 1.- Concluded.

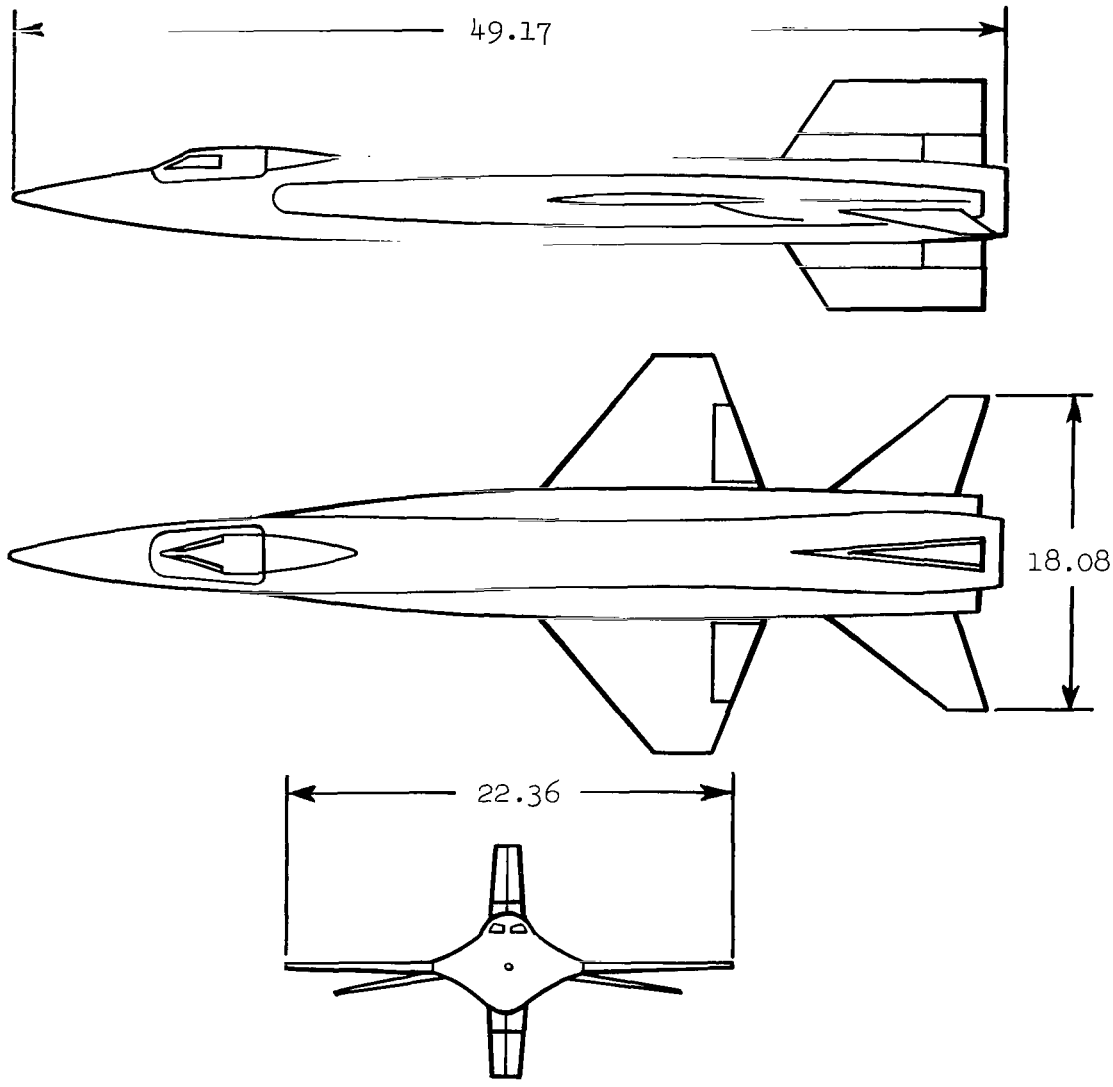

Figure 2.- Three-view drawing of X-15 airplane. Dimensions in feet.

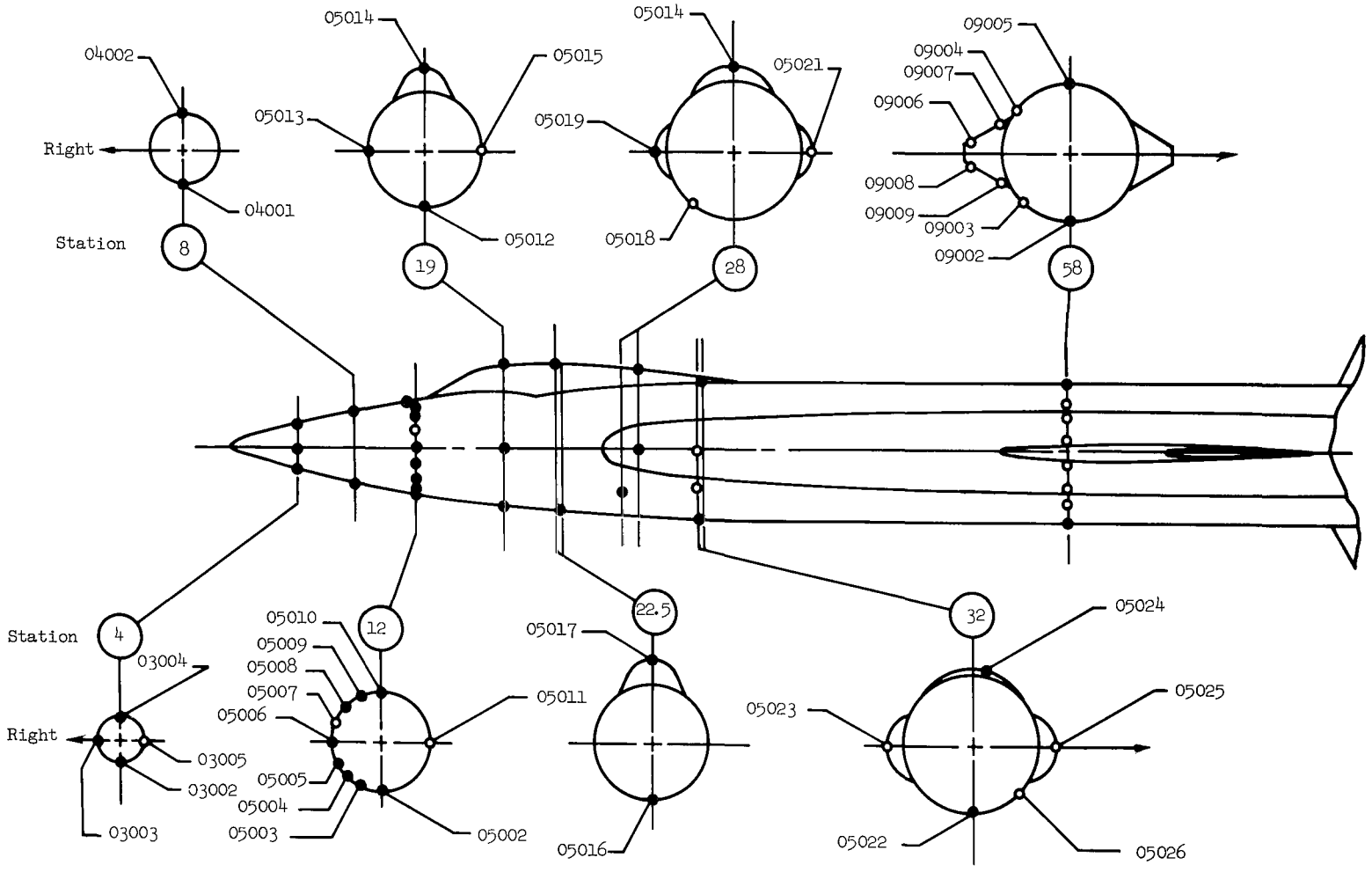

Figure 3.- Surface pressure-orifice locations on the X-15 fuselage. Solid circles indicate orifices used in this investigation. Stations are shown in percent fuselage length.

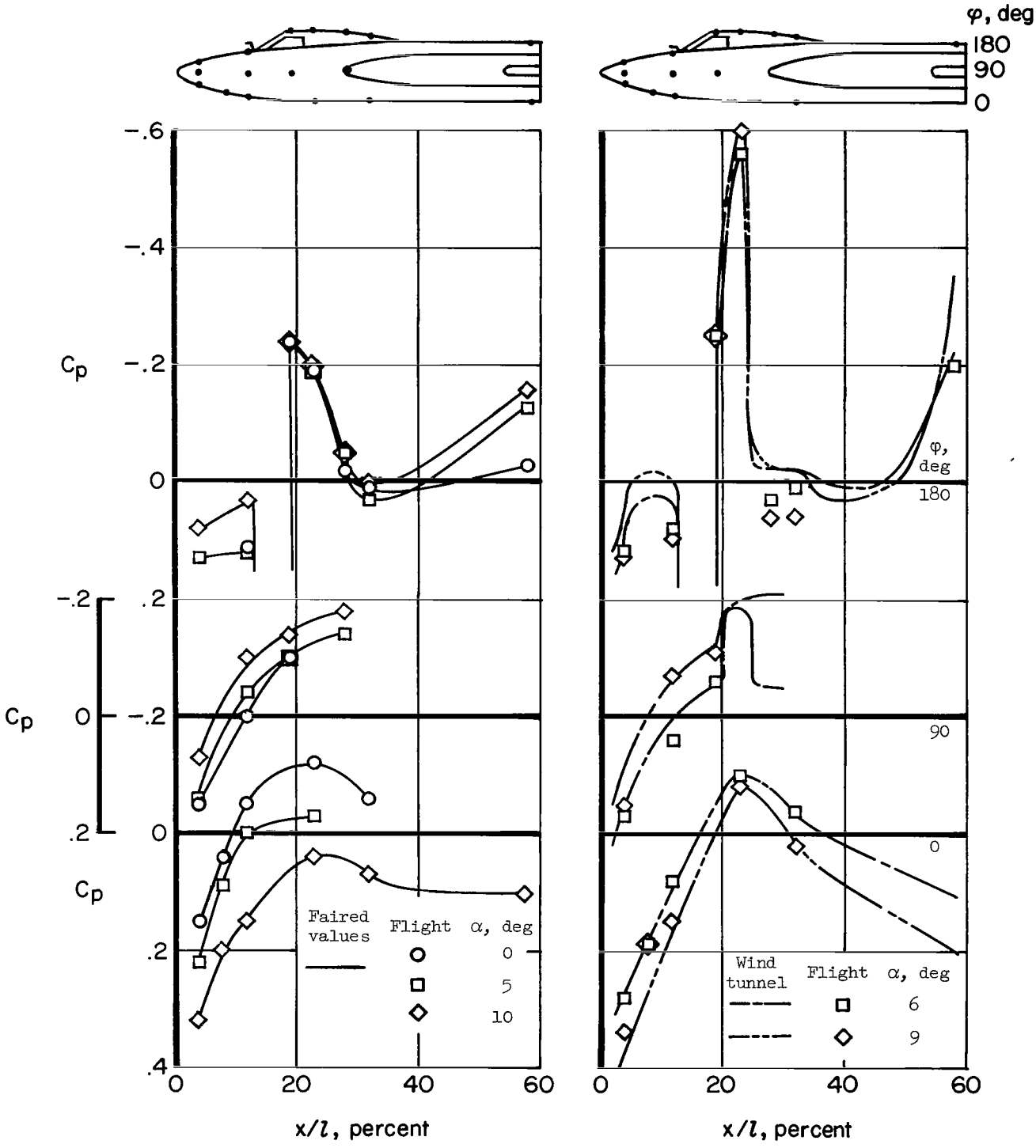

(a) M = 0.8.

(b) M = 0.9.

Figure 4.- Surface pressure distributions along the X-15 fuselage and comparison with wind-tunnel measurements.

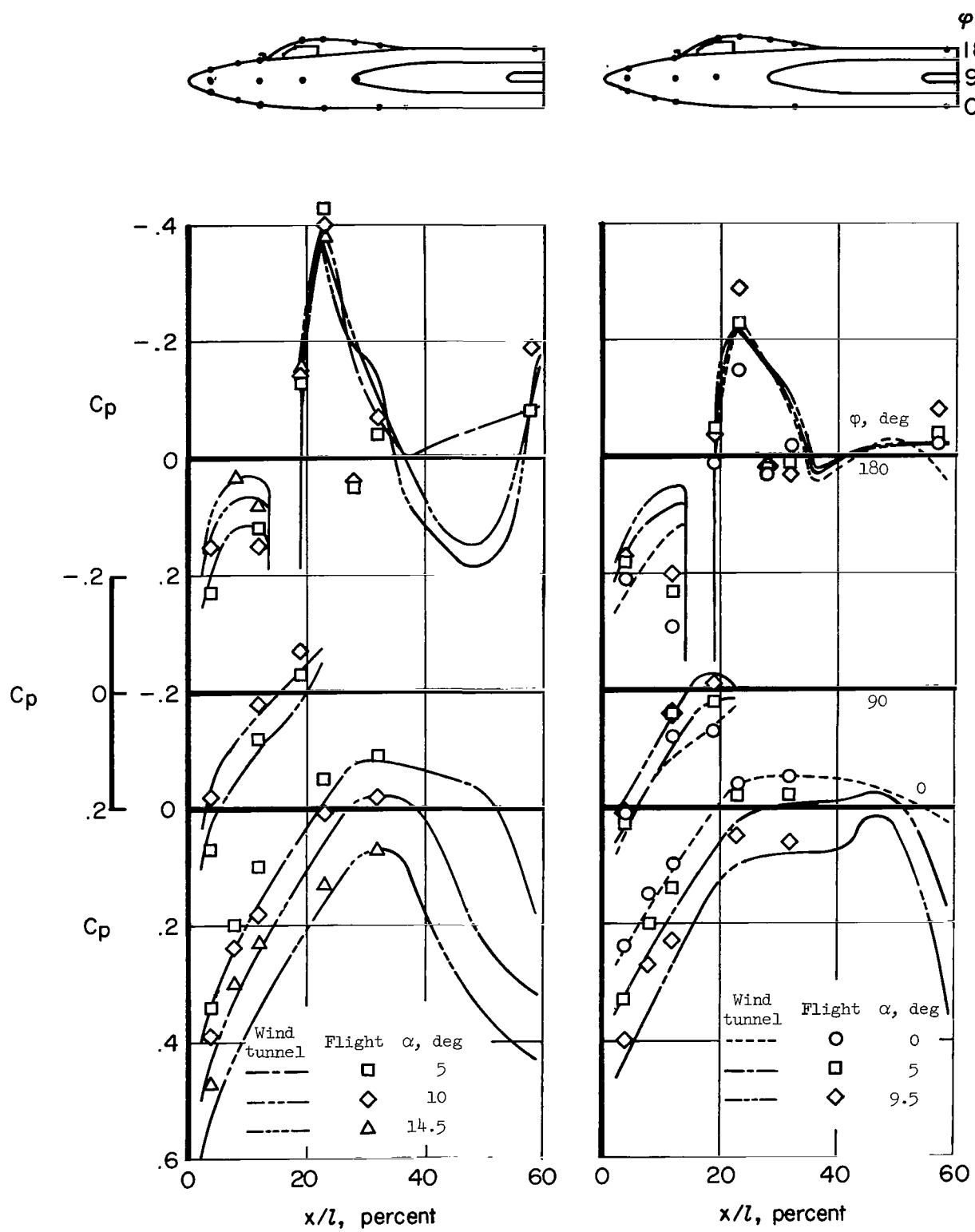

Figure 4.- Continued.

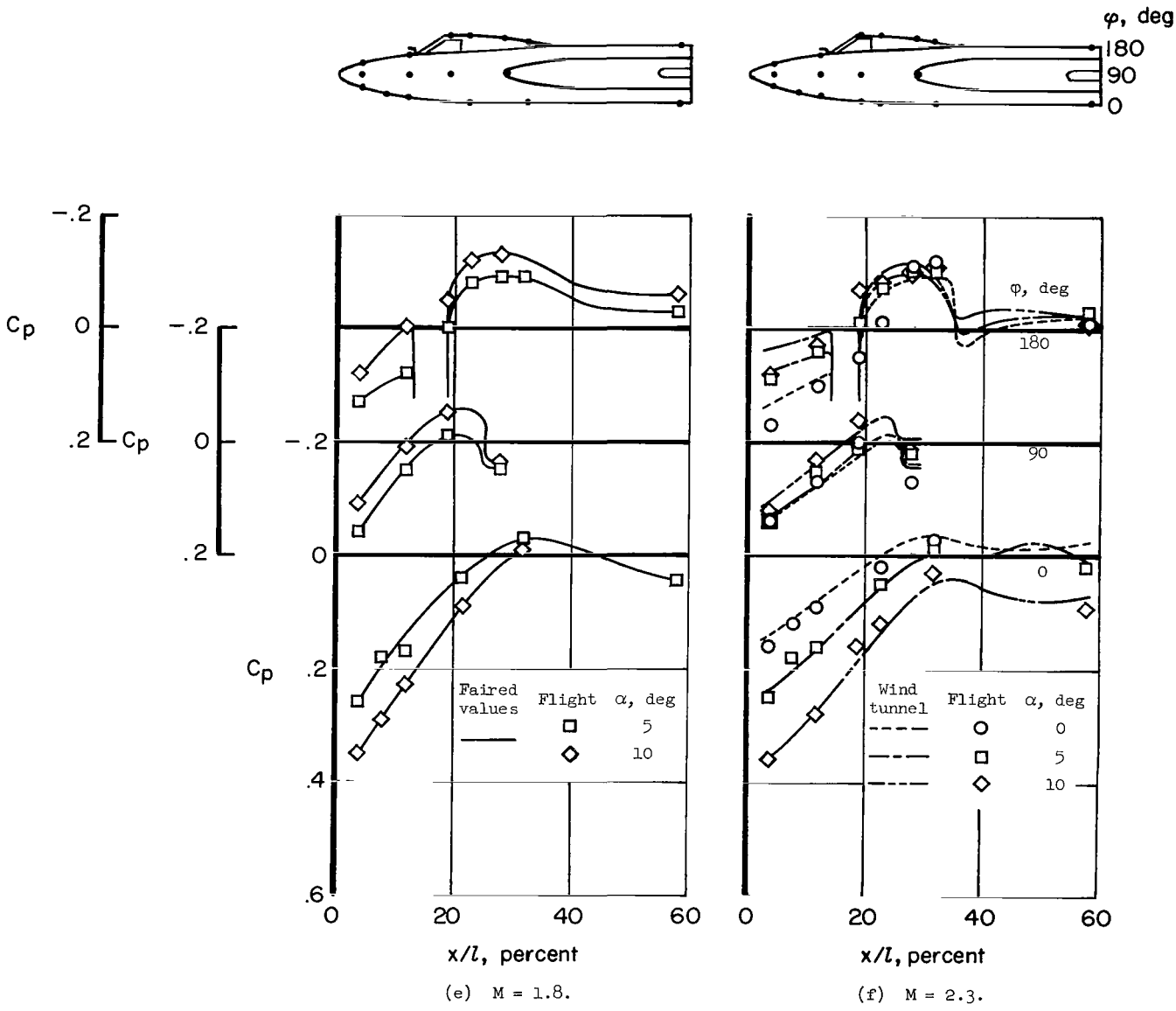

(e) M = 1.8.

(f) M = 2.3.

Figure 4.- Continued.

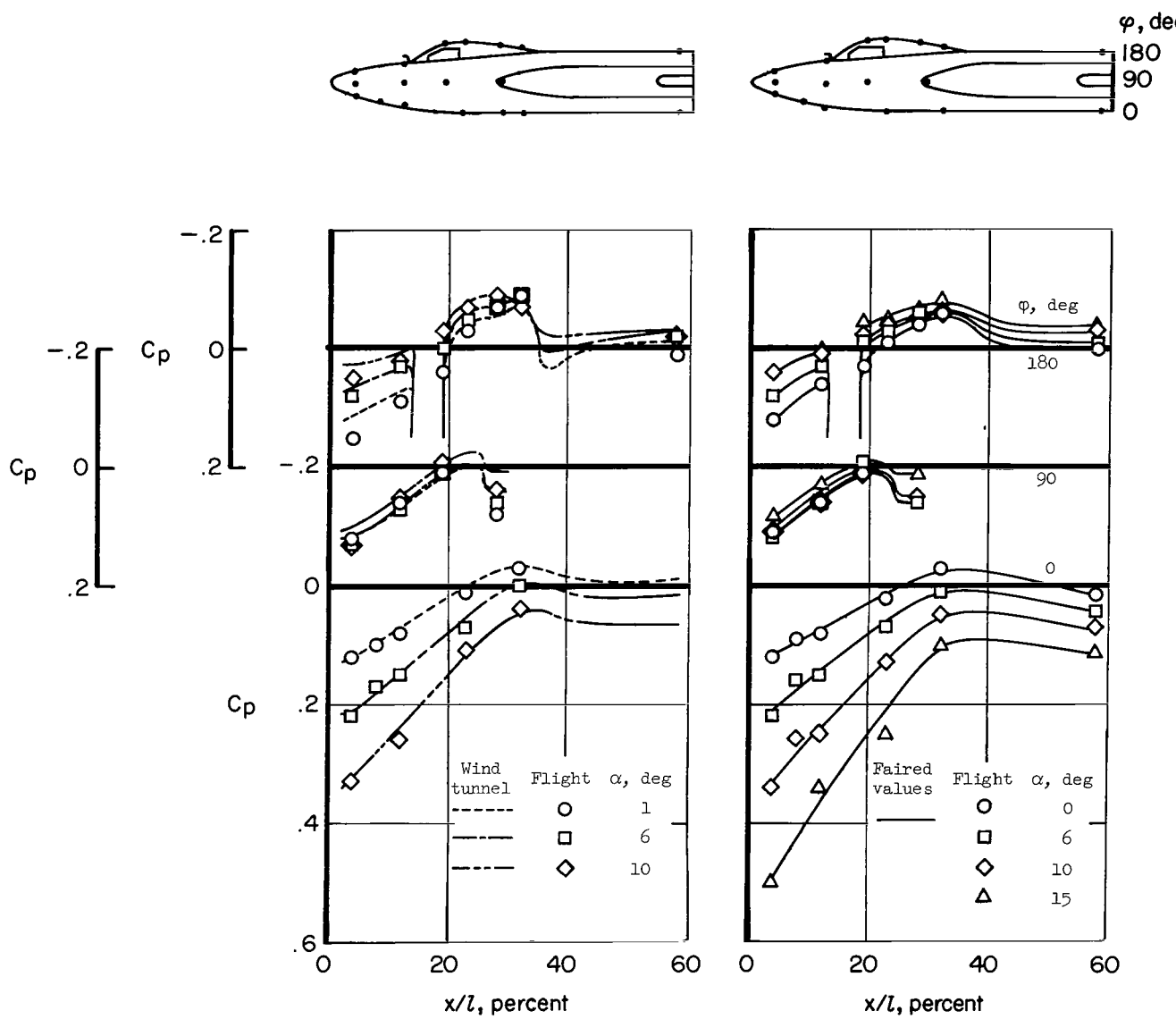

(g) M = 3.0.

(h) M = 4.0.

Figure 4.- Continued.

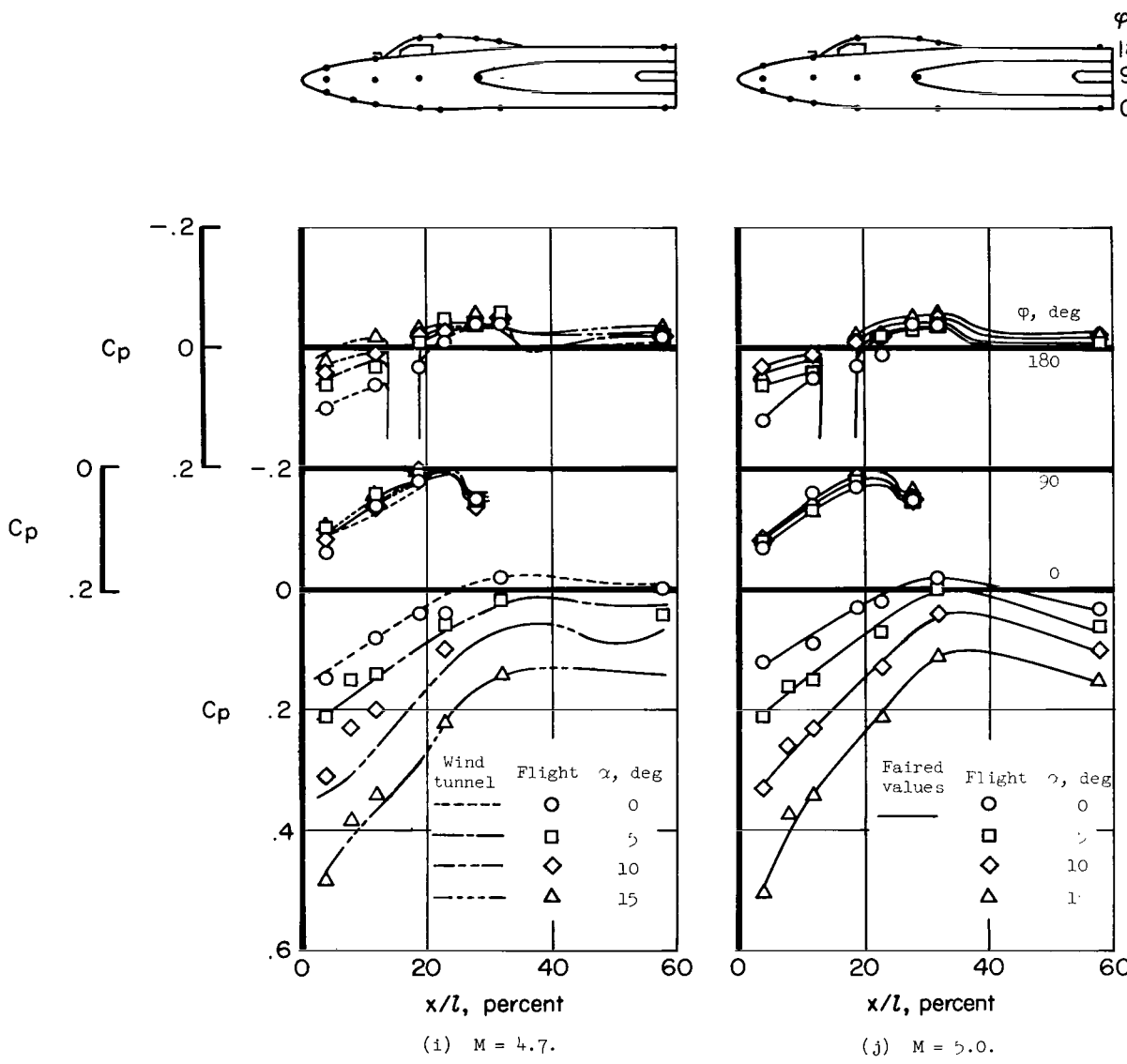

(i) M = 4.7.

(j) M = 5.0.

Figure 4.- Continued.

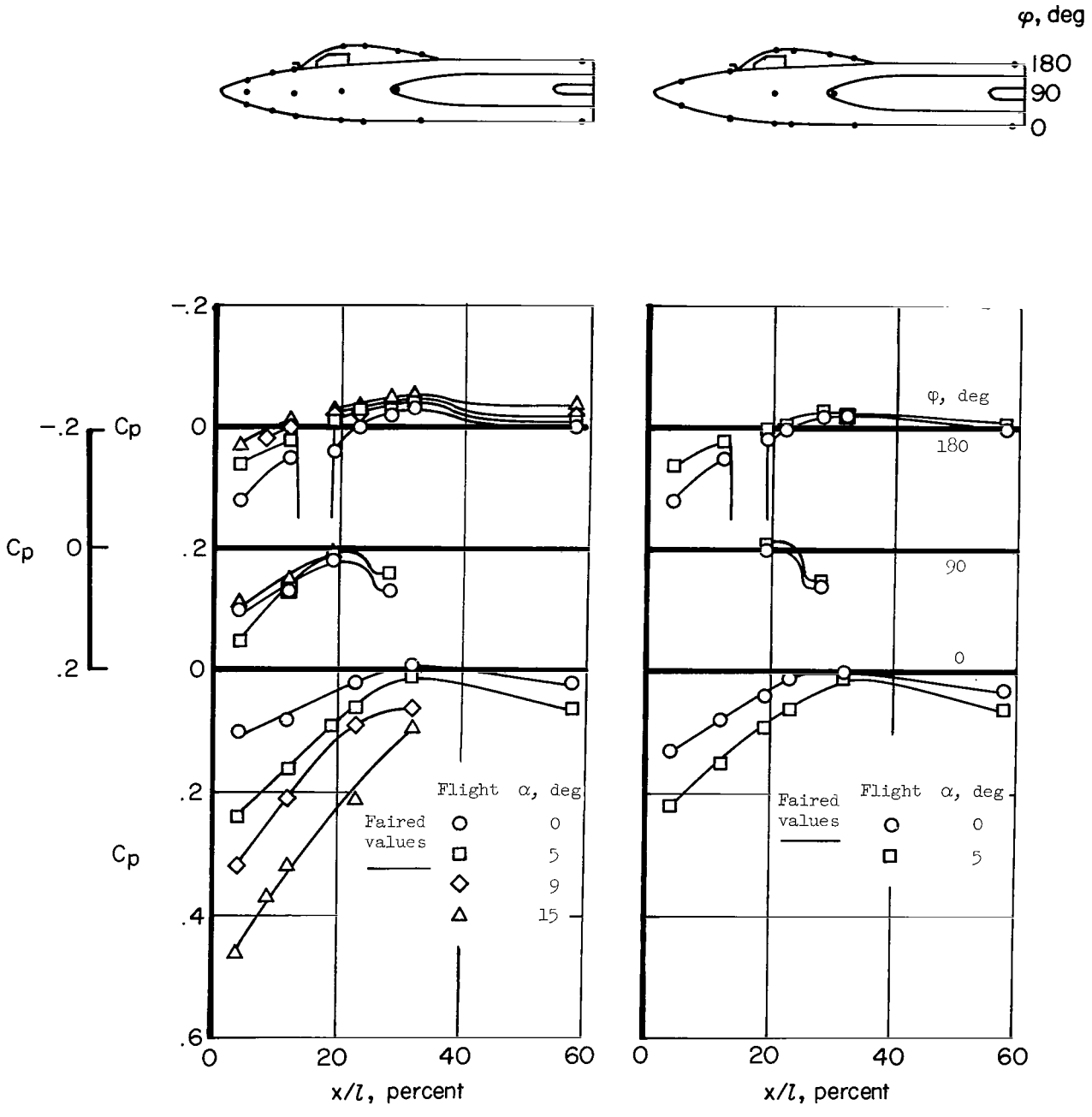

Figure 4.- Concluded.

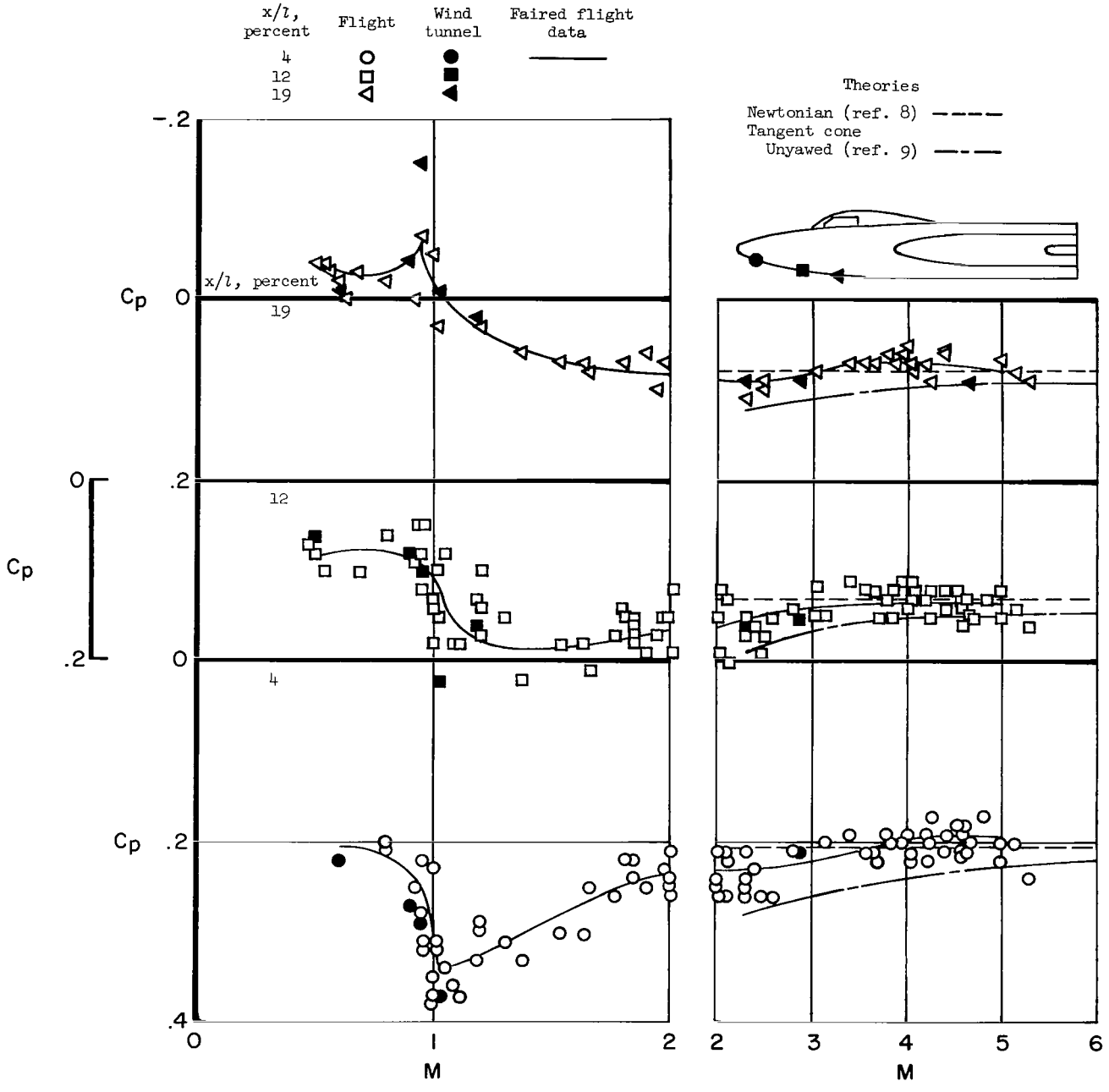

(a) $\alpha = 4°$ to $6°$.

Figure 5.- Effect of Mach number on the pressure coefficient at three points along the bottom centerline of the X-15 fuselage, and comparisons with wind-tunnel results and theory.

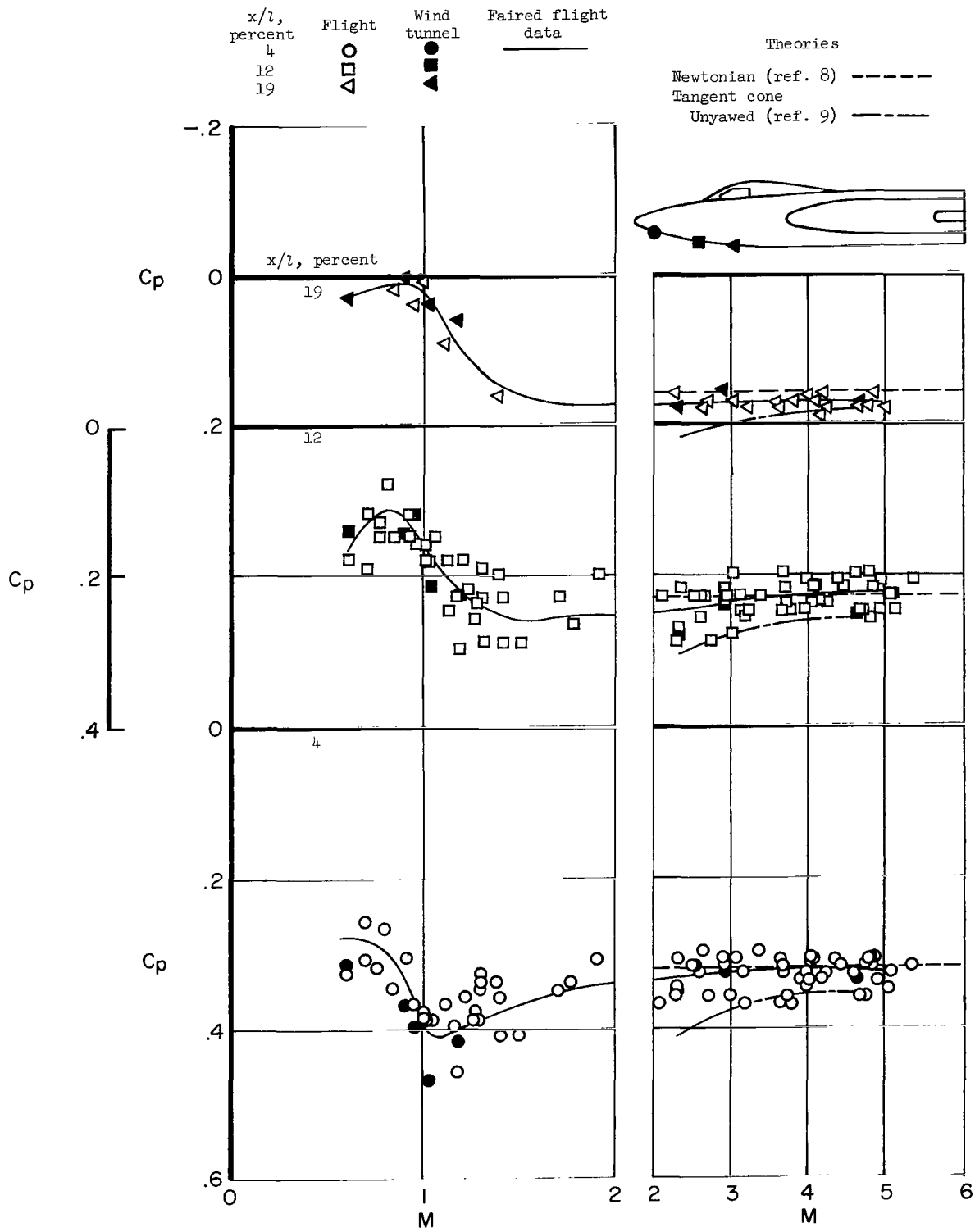

(b) $\alpha = 9°$ to $11°$.

Figure 5.- Concluded.

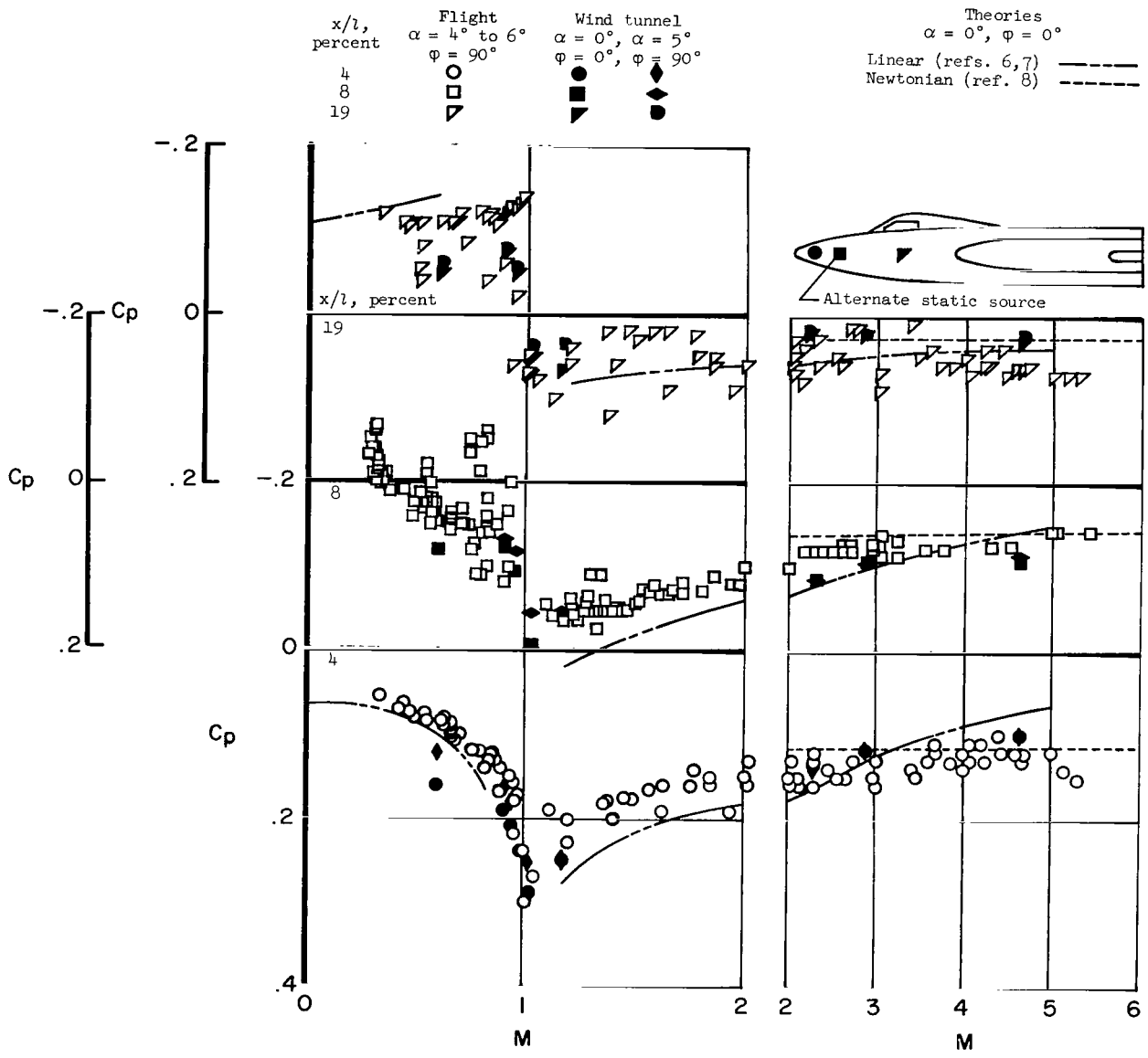

Figure 6.- Comparison of flight data with results from wind-tunnel test and theory for several points along the forward side of the X-15 fuselage forebody (φ = 90°).

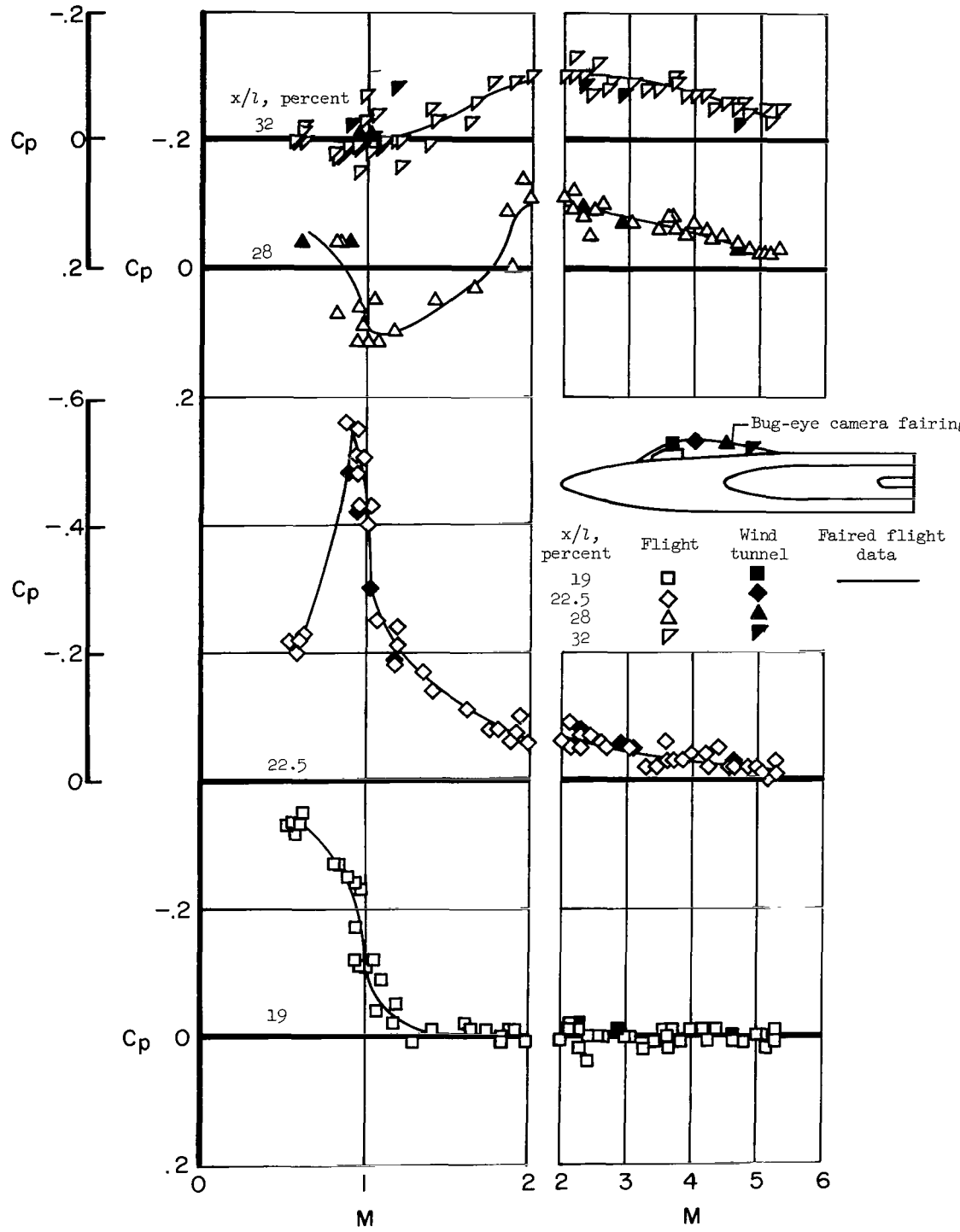

(a) $\alpha = 4°$ to $6°$.

Figure 7.- Effects of Mach number on the pressure coefficients for the canopy centerline on the X-15 airplane.

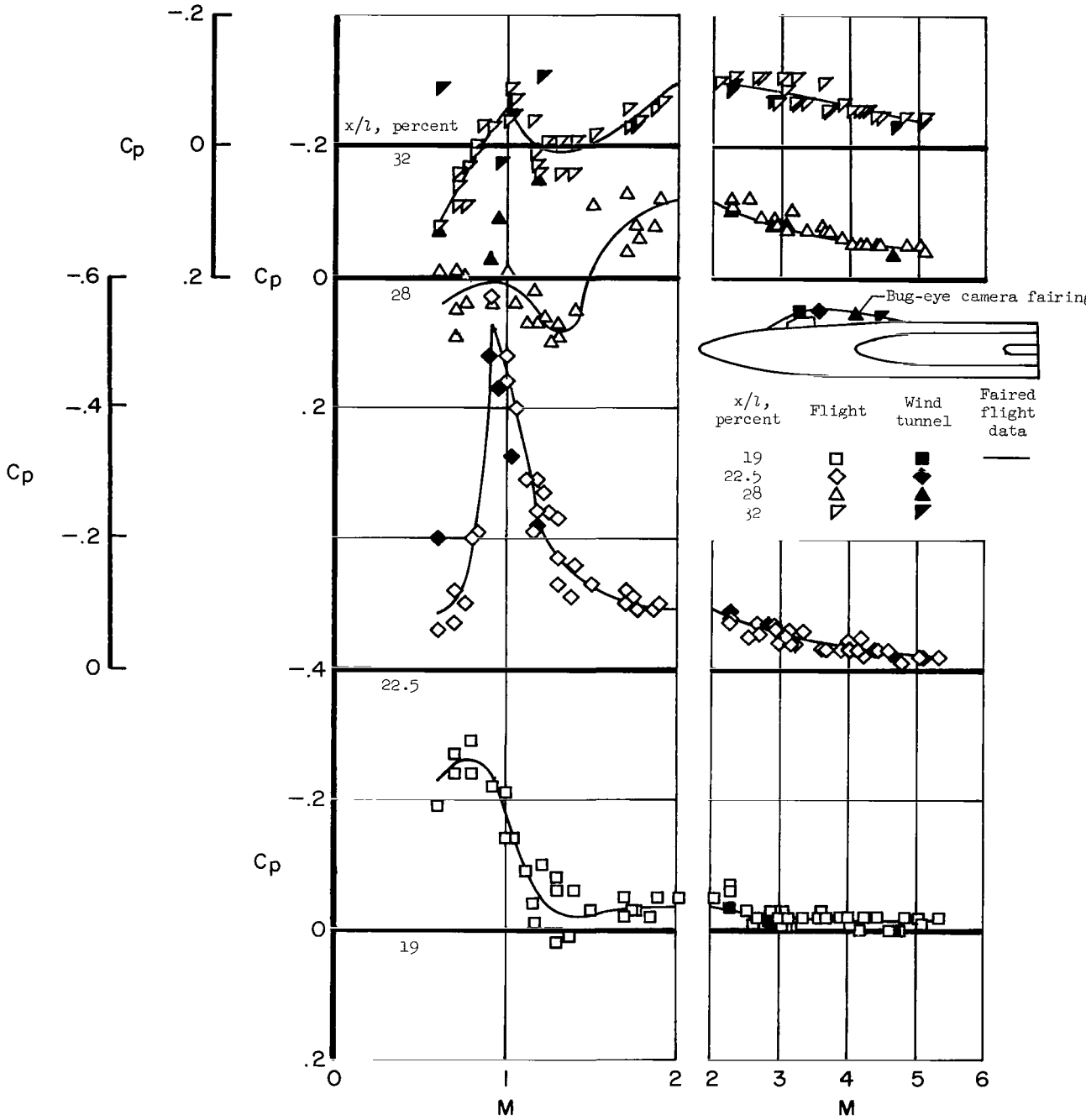

(b) $\alpha = 9°$ to $11°$.

Figure 7.- Concluded.

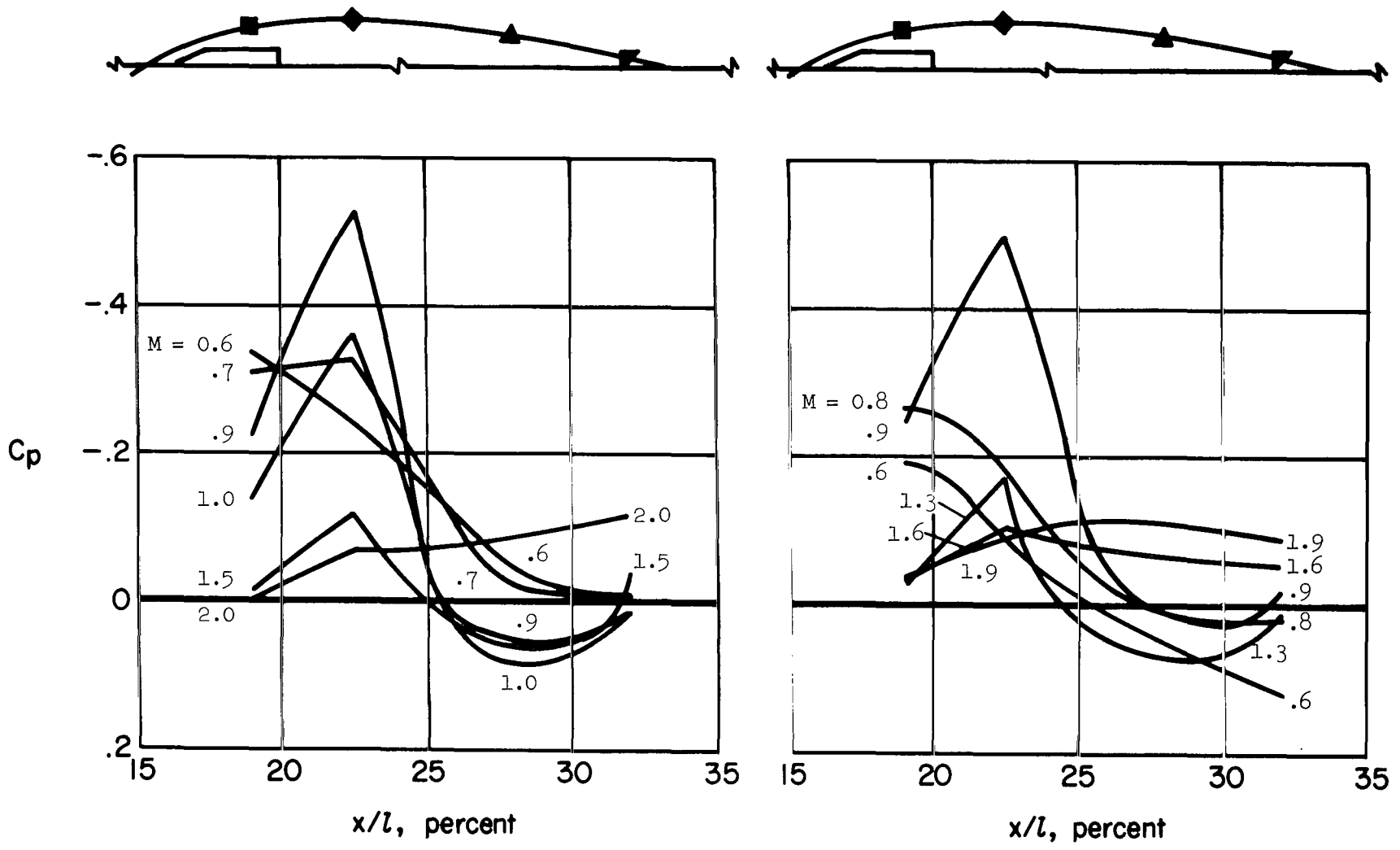

(a) $\alpha \approx 5°$.

(b) $\alpha \approx 10°$.

Figure 8.- X-15 canopy pressure distribution for several transonic Mach numbers at angles of attack of approximately 5° and 10°.

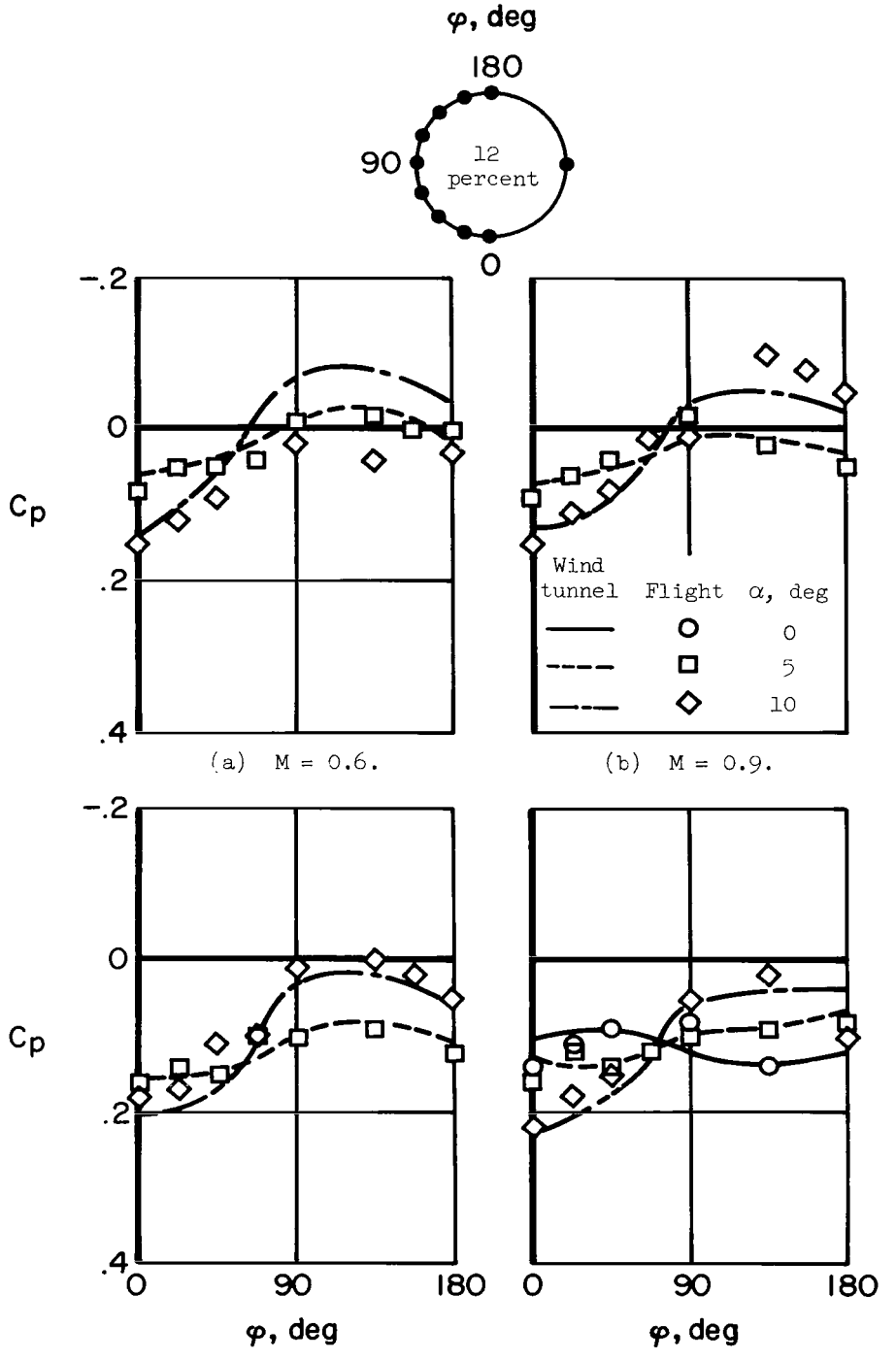

Figure 9.- Comparison of flight-determined radial pressure distributions at the 12-percent location of the X-15 fuselage with interpolated wind-tunnel results.

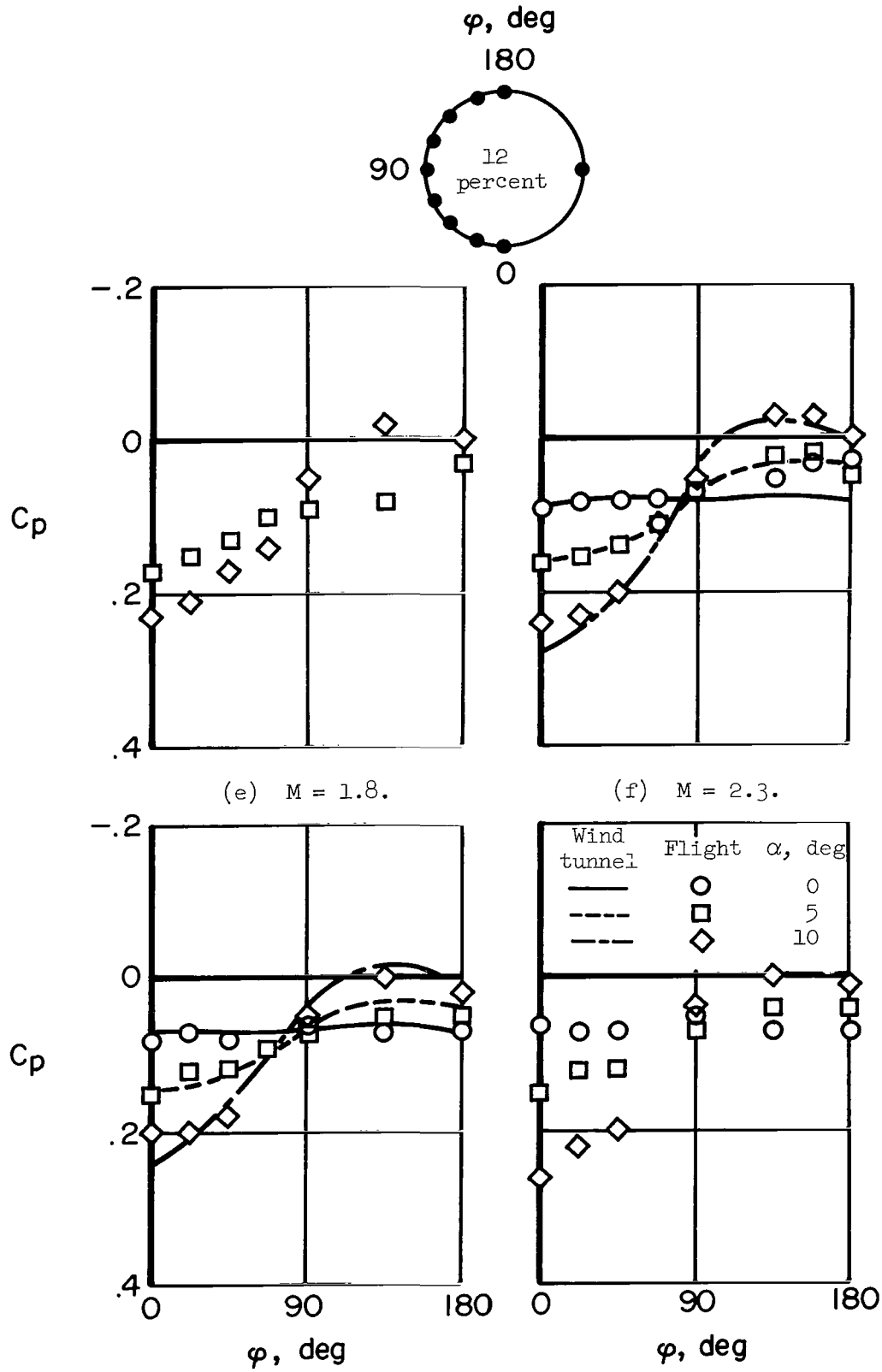

(e) M = 1.8.

(f) M = 2.3.

(g) M = 3.0.

(h) M = 4.0.

Figure 9.- Continued.

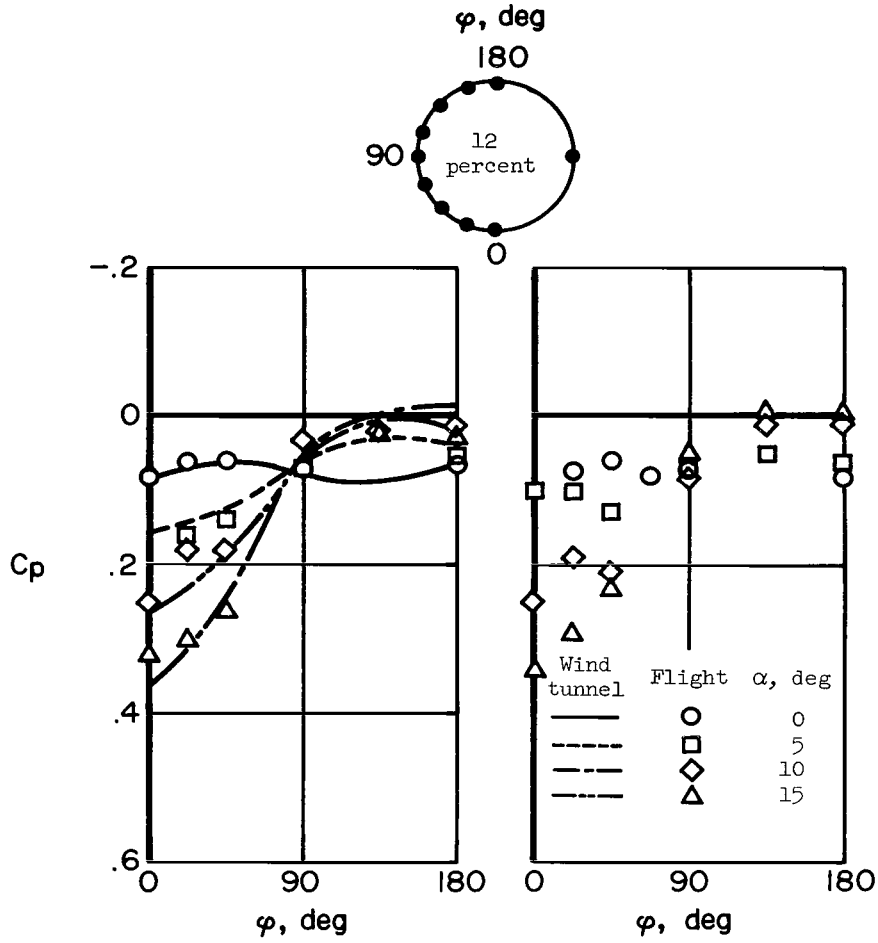

(i) M = 4.7. (j) M = 5.0.

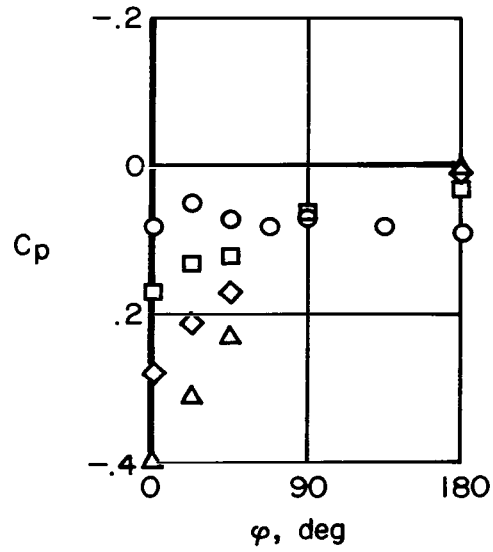

(k) M = 5.5.

Figure 9.- Concluded.

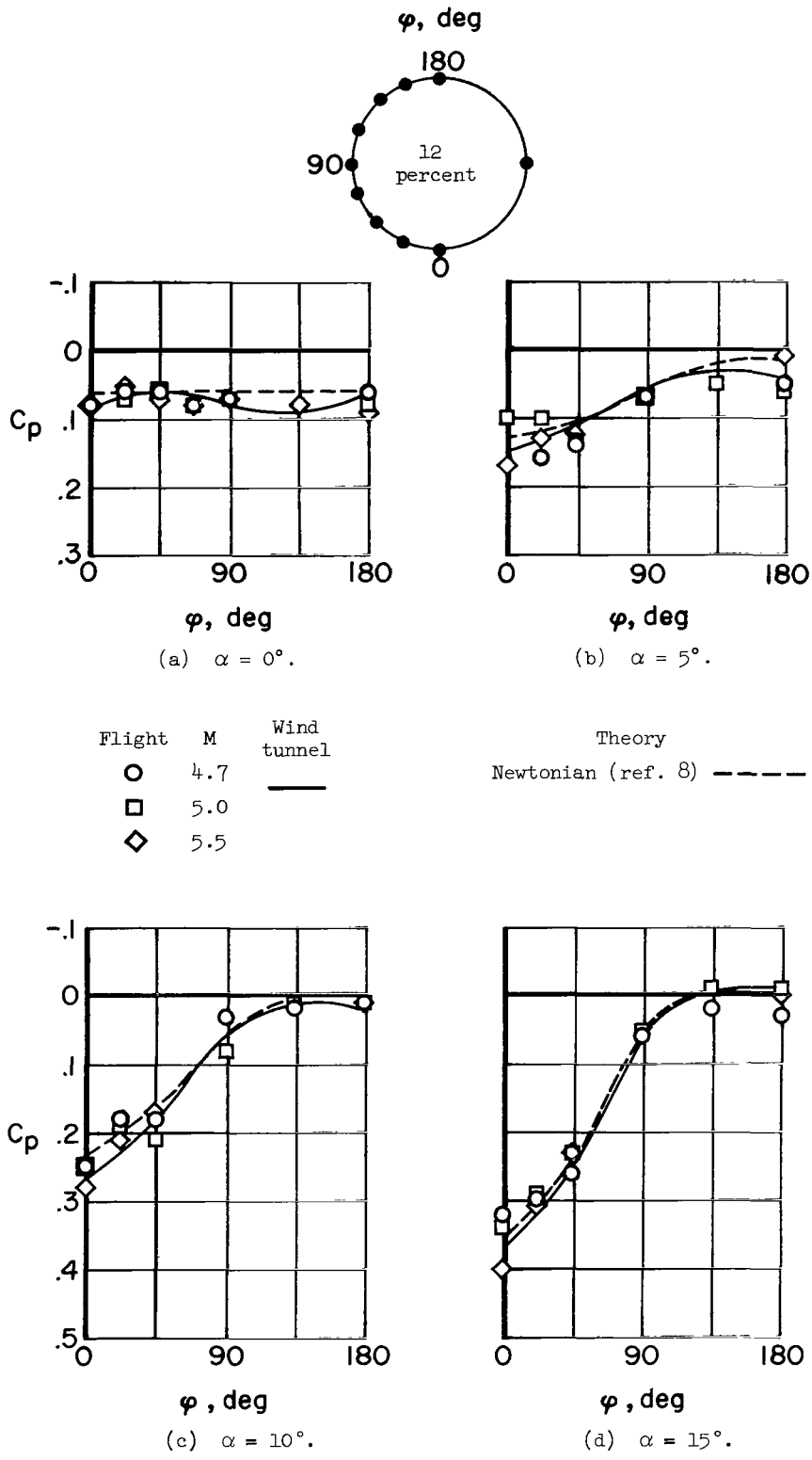

Figure 10.- Comparison of flight-determined radial pressure distributions (12-percent fuselage length) at supersonic speeds with wind-tunnel results and theory.

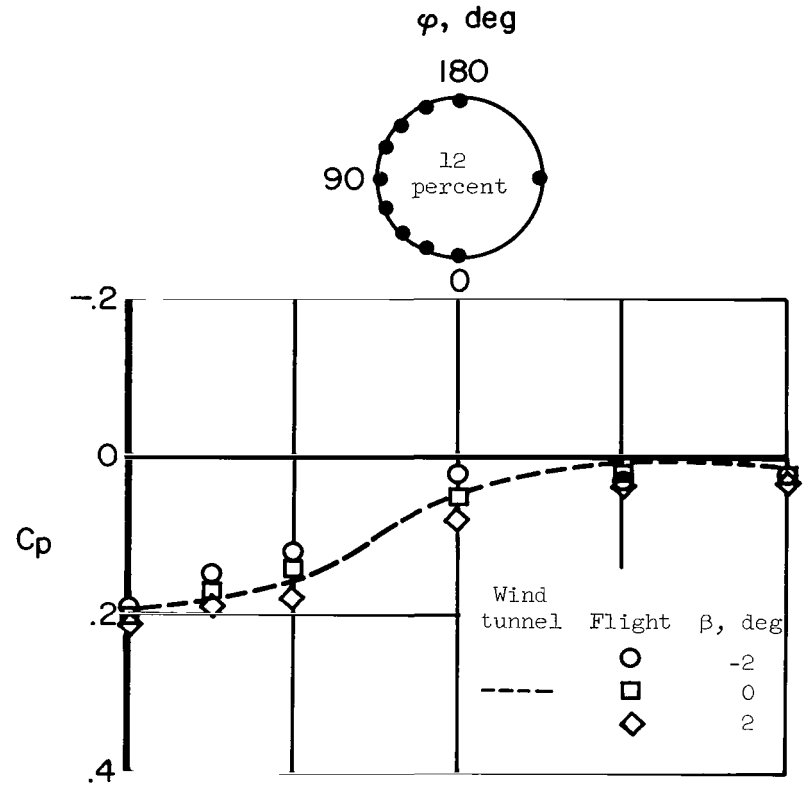

(a) M = 2.8, α = 7°.

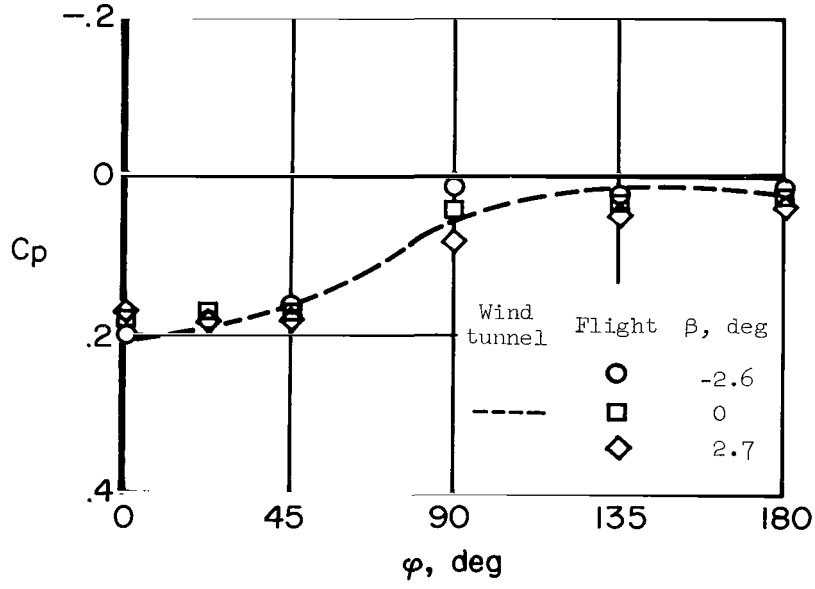

(b) M = 3.8, α = 8°.

Figure 11.- Effect of sideslip on the X-15 radial pressure distributions at the 12-percent fuselage station.